Network analysis of ChIP-seq data by VULCAN identifies GRHL2 as a key co-regulator of ERa in luminal breast cancer

Andrew N. Holding[1,2,5,*], Federico M. Giorgi[1,3,5], Amanda Donnelly[1], Amy E. Cullen[1], Sankari Nagarajan[1], Luke A Selth[4], and Florian Markowetz[1]

[1] CRUK Cambridge Institute, University of Cambridge, Robinson Way, Cambridge, CB2 0RE
[2] The Alan Turing Institute, 96 Euston Road, Kings Cross, London NW1 2DB
[3] Department of Pharmacy and Biotechnology, University of Bologna, Via Selmi 3, Bologna, Italy
[4] Dame Roma Mitchell Cancer Research Laboratories and Freemasons Foundation Centre for Men's Health, Adelaide Medical School, The University of Adelaide, SA, Australia

[5]These authors contributed equally to this work.

*Corresponding Author

Abstract

VULCAN infers regulatory interactions of transcription factors by overlaying networks generated from tumor expression data onto ChIP-seq data. VULCAN analysis of estrogen receptor (ER) activation in breast cancer highlighted key components of the ER complex alongside a novel interaction with GRHL2. We demonstrate that GRHL2 is recruited to a subset of ER binding sites and regulates the transcriptional output of ER, as evidenced by: changes in ER-associated eRNA expression; and stronger ER binding at active enhancers (H3K27ac sites) after GRHL2 knockdown. Our findings provide new insight into ER signaling and demonstrate VULCAN, available from Bioconductor, as a powerful predictive tool.

100/100

Keywords: Breast Cancer, Network Analysis, Dynamics, ER, Master Regulator, ChIP-seq, VULCAN, GRHL2, P300, H3K27ac

Introduction

Breast cancer is the most common form of cancer in women in North America and Europe accounting for 31% of all new cancer cases. In the US, it is estimated that 41,400 deaths will have occurred from the disease in 2018 [1]. The majority of breast cancers, approximately 70%, are associated with deregulated signaling by the Estrogen Receptor-alpha (ER), which drives tumor growth. Therefore, in ER-positive (ER+) tumors, ER is the primary therapeutic target. During activation, ER recruits several cofactors to form an active complex on the chromatin. FOXA1 is of particular interest as the protein shares nearly 50% of its genomic binding sites with ER and has been shown to operate as a pioneer factor before ER activation [2], [3]. It is through FOXA1 and other cofactors (e.g SRC-1) [4], [5], that ER is able to recruit RNA Polymerase II at the gene promoter sites by way of adaptor proteins in order to initiate transcription [6]. Combinatorial treatments targeting ER cofactors present a significant opportunity in breast cancer therapy for increasing patient survival. In particular, the pioneer factor FOXA1 [7] has been identified as novel therapeutic target for the treatment of breast cancer, while the EZH2-ERα-GREB1 transcriptional axis has been shown to play a key role in therapeutic resistance [8].

ChIP-seq enables the identification of potential site-specific interactions at common binding sites between transcription factors and their cofactors; however, to fully characterize all potential cofactors of a single project on this scale is laborious and expensive. To follow up all potential cofactors identified by a chromatin-wide proteomics method, e.g. RIME [9] or ChIP-MS [10], would take hundreds of individual ChIP-seq experiments. Studies like ENCODE [11] have gone a long way to provide a resources to meet these challenges; however, the inherent scale of the

problem means public studies can only offer data for a subset of TF in a limited number of models. For a single lab to undertake this level of experimentation is unfeasible, and in cases where suitable antibodies for the ChIP do not exist, impossible.

To enable discoveries beyond collections like ENCODE, we are proposing a computational framework to integrate patient data in the the prediction of functional protein-protein interactions. By applying machine learning methods, we are able to surpass the limitation of current predictive tools that exist to support the interpretation of data. Previous methods provide information in the context of predefined biological pathways and established gene sets [12], [13] or through motif analysis [14], while our method is built on data specific to the disease being studied.

Our method, "**V**irt**U**a**L** **C**hIP-seq **A**nalysis through **N**etworks" (VULCAN), is able to specifically analyze potential disease-specific interactions of TFs in ChIP-seq experiments by combining machine learning approaches and patient data. Previously, the strategies employed by VULCAN were limited to the analysis of transcription data. By developing VULCAN to overlay coexpression networks established from patient tumor data onto ChIP-seq data, we are able to provide candidate coregulators of the response to a given stimulus (**Figure 1**). Further, as VULCAN builds on transcriptional master regulator analysis, the output from the pipeline provides the end user with functional information in terms of the activity of potentially interacting TFs. The combination of disease-specific context and TF activity information presents a significant step forward in providing valuable information for the elucidation of on-chromatin interactions from ChIP-seq experiments over previous strategies.

Through the application of VULCAN to the activation of the ER in breast cancer, we were able to identify multiple previously characterized cofactors of the ER along with GRHL2 as a potential co-repressor of the ER. We then demonstrated experimentally that GRHL2 is able to modulate the expression of eRNA at ER bound enhancers, and the removal of the P300 inhibitory alpha-helix results in suppression of the inhibitory effect on eRNA production.

Results

In the following, we first benchmark VULCAN's performance in a comprehensive comparison to alternative approaches. We then apply it to our data on temporal ER binding, which identifies GRHL2 as a novel ER cofactor and we explore its function.

Comparison of VULCAN to existing methods

Mutual Information networks outperform Partial Correlation networks

We generated a mutual information network with ARCANe alongside several partial correlation networks at different thresholds all from the TCGA Breast Cancer data. To ensure robustness of our method, we tested the overlap of every partial correlation network with the mutual information network using the Jaccard Index (JI) criterion (**Suppl. Figure S2-28**). Finally, we showed how the Jaccard Index between partial correlation networks and the ARACNe network is always significantly higher than expected by selecting random network edges (**Suppl. Figure S2-29**). For further analysis, we selected the mutual information network generated by ARACNe as this method outperformed partial correlation networks at all thresholds.

GSEA is the optimum method for VULCAN's target enrichment analysis

VULCAN applies Gene Set Enrichment Analysis [15] to identify enrichment of our mutual information network derived regulons in differential ChIP-seq data. To validate our method, we compared the results of VULCAN when applied to our ER binding data against three independent methods previously applied to benchmark VIPER [16]. The first implemented a Fisher p-value integration step. This test lacks stringency and results in nearly all regulons as significantly enriched (**Suppl. Figure S2-30**). Second, we implemented a fraction of targets method, defining for every TF the fraction of their targets that are also differentially bound. This alternative to VULCAN ignores the MI strength of interaction and the individual strengths of differential bindings, reducing the resolving power of the algorithm (**Suppl. Figure S2-31**). Finally, we compared to a Fisher's Exact Method, which assesses the overlap between networks and significant differential binding. This method is too stringent (as observed in the original VIPER paper) [16]; and even without p-value correction, there are no significant results, even at low stringency, demonstrating the low sensitivity of using a Fisher's Exact Method method (**Suppl. Figure S2-32**). In summary, VULCAN GSEA implementation outperformed all three alternative methods we tested (t-test based; fraction of targets method; and Fisher's Exact Method) in our dataset and was therefore applied to all downstream analysis of ChIP-seq data.

VULCAN outperforms enrichment analysis tools (GREAT, ISMARA & ChIP-Enrich)

To further validate our method, we compared the output of our GSEA analysis with different versions of promoter-enrichment approaches implemented by GREAT [12], ISMARA [14] and ChIP-Enrich [13]. The VULCAN analysis shows a significant overlap in terms of detected pathways with the GREAT method (**Suppl. Figure S2-33**). ChIP-Enrich identifies enrichment of a number of TFs also predicted by VULCAN, but it fails to identify ESR1 as the top transcription factor affected by our experiment (**Suppl. Figure S2-34**). ISMARA succeeds at identifying ESR1

using a motif-based analysis, but does not identify other candidate binding TFs (**Suppl. Figure S2-35**). In summary, VULCAN outperforms both ISMARA and ChIP-Enrich, and significantly overlaps with GREAT, but provides additional value through inference of TF factor activity.

Temporal analysis of ER DNA binding profiles after activation by E2

We performed four replicated ChIP-seq experiments for ER at three time points (0, 45 and 90 minutes) after estradiol treatment **(Figure 2)** in the ER+ breast cancer cell line, MCF7**.** The cistromic profile of ER at 45 and 90 minutes was then compared to 0 minutes to identify binding events enriched by E2. Our analysis (**Figure 2B,C**) identified 18,900 statistically significant binding events at 45 minutes (FDR < 0.05) and 17,896 numbers at 90 minutes. We validated the ER binding behavior with ChIP-qPCR (**Figure 2A**) and the response was sustained, in agreement with our previous study [17]

We performed motif enrichment analysis (HOMER software) on ER binding sites detected by differential binding analysis. Our analysis confirmed a strong enrichment for a single element, ERE, bound at both 45 and 90 minutes, with a corrected p-value of 0.0029 (**Figure 3F**). When clustered according to peak intensity, samples cluster tightly in two groups: treated and untreated (**Suppl. Figures S2-1, S2-2 and S2-3**), but treatment at 45 and 90 minutes is detectably different on a genome-wide scale, as highlighted by Principal Component Analysis (**Suppl. Figures S2-4 and S2-5**).

We performed a Gene Set Enrichment Analysis (GSEA) [15] and an associated Rank Enrichment Analysis (aREA) [16] using the differential binding at gene regulatory regions with time 0 as reference. Individual differential binding signatures for GSEA were calculated using a negative

binomial test implemented by DiffBind [18]. The collective contribution of differentially bound sites highlights several ER-related pathways in both the GSEA and aREA analyses [19]–[21] (**Suppl. Figure S2-22**). The strongest upregulated GSEA pathway in both time points (**Table S2 and S5**) was derived from RNA-seq in an MCF7 study using estradiol treatment [20], confirming the reproducibility of our dataset.

VULCAN analysis of ER activation

VULCAN identifies coactivators and corepressors of ER

We leveraged the information contained in mutual information networks to establish TF networks enriched in the differential binding patterns induced by estradiol. From our analysis of ER binding, we established four classes of modulation: early coactivators, early corepressors, delayed coactivators and transient coactivators (**Figure 3**).

Using VULCAN, we defined TF network activity of occupied regulatory regions (**Figure 3A**) according to the binding of ER within their promoter and enhancer regions (limited to 10kb upstream of the Transcription Starting Site to ensure gene specificity). We define early coactivators as those TFs whose network is upregulated at both 45 and 90 minutes (**Figure 3B**); these genes include AR, SP1 and CITED1. TFs with opposite behavior (namely TFs whose negative/repressed targets in the ARACNe model are occupied by ER), or “early corepressors”, include GLI4, MYCN and GRHL2 (**Figure 3C**). Some TFs appear to have their targets transiently bound at 45 minutes, but then unoccupied at 90 minutes and therefore we dubbed them “transient coactivators’ (**Figure 3D**). We further defined TFs active at 90 minutes but not at 45 minutes as “delayed coactivators”, noting these cofactors could be the transient if the response is not completed by 90 minutes. While this category exists, and notably contains both ESR1 and the

known ESR1 interactor GATA3, it is just below the significance threshold at 45 minutes (**Figure 3E**).

We repeated our TF network activity analysis of ER activation (**Figure 3A-E**) on an independent dataset from TCGA and found similar results to those established from the METABRIC-derived network (**Suppl. Figures S2-14 to S2-18**).

To ensure the robustness of the results, we performed a joint analysis of data obtained from both networks. At 45 (**Figure 4A**) and 90 minutes (**Figure 4B**) we identified candidates, specifically the ESR1, GATA3 and RARA networks, which were consistently and robustly activated by ER in both time points. The joint analysis also identified candidate corepressors, including HSF1 and GRHL2.

VULCAN results are specific to the cancer used for network modeling

As a negative control, we used a different context ARACNe network, derived from the TCGA acute myeloid leukemia (AML) dataset. This network shows globally weaker enrichment scores and a weak positive correlation with the results obtained through breast cancer regulatory models (**Suppl. Figure S2-21**).

VULCAN is able to predict protein-protein interactions in both patient-derived xenografts (PDX) and prostate cancer

To demonstrate the general applicability of VULCAN, we applied the algorithm to a Breast Cancer Patient-derived xenograft dataset (Gene Expression Omnibus series GSE110824) [22], [23], which showed the expected enrichment of the ESR1, FOXA1 and GATA3 regulons (**Suppl.**

Figure S2-36 and Figure 5A) predicting the colocalization of the respective proteins on the chromatin. To further test the generality of VULCAN, we applied the method to another cancer-associated transcription factor type. More specifically, we evaluated an androgen receptor ChIP-seq dataset derived from prostate cancer cell line model LNCaP-1F5 and VCaP (Gene Expression Omnibus Series GSE39880, AR + DHT, RU486 or CPA) [24]. By applying a context specific network built from the TCGA prostate cancer dataset, we could predict functional colocalization of FOXA1 and AR in target genes' promoters after dihydrotestosterone (DHT) treatment in prostate cell lines (**Suppl. Figure S2-37 and Figure 5B**), validating the known role of FOXA1 in AR-regulated gene transcription in prostate cancer [25][26][27]

VULCAN outperforms classical motif analysis

Finally, we compared VULCAN to a classical motif analysis by exploiting the MsigDB C3 collection v6.1 [28] of gene sets, which contain canonical TF-specific binding motifs in their promoters. Our analysis shows the correlation of VULCAN results for two transcription factors (e.g. between GATA3 and ESR1, **Suppl. Figure S2-38**) can be relatively high but not significantly overlapping in terms of target genes containing the same canonical motifs (**Suppl. Figure S2-39**). We could prove that this non-relationship is general as it extends to the majority of TF-TF pairs that were present in the MsigDB database (**Suppl. Figure S2-S40**).

GRHL2 is a novel ER cofactor

In our analysis of ER dynamics, the GRHL2 transcription factor was consistently identified as a key player, using both the METABRIC and TGCA networks. GRHL2 is a transcription factor that is important for maintaining epithelial lineage specificity in multiple tissues [29], [30]. It has previously been predicted to exist in ER-associated enhancer protein complexes [31], but its

function in the ER signaling axis is unknown. Therefore, we set out to experimentally validate GRHL2 as an ER cofactor.

There is only a weak, positive correlation between ESR1 and GRHL2 expression in the TCGA and METABRIC breast cancer datasets (**Suppl. Figure S2-25**). Furthermore, GRHL2 does not change significantly in different PAM50 subtypes, although it is overexpressed in malignant tissue. The low correlation between GRHL2 expression and subtype implies that the protein is controlled by mechanisms such as phosphorylation [32], subcellular localization or on-chromatin protein-protein interactions.

qPLEX-RIME detects a significant increase in the ER-GRHL2 interaction on activation

We undertook a complementary, unbiased, experimental approach combining RIME [9] with TMT [33], called qPLEX-RIME [34], to identify interactors of ER within the ER-chromatin complex. We generated ER qPLEX-RIME data from MCF7 cells treated with estradiol at both 45 and 90 minutes and compared this to the VULCAN dataset (**Suppl. Figure S2-27**). We found known ESR1 interactors with both methods, namely HDAC1, NCOA3, GATA3 and RARA. These interactors have positive enrichment according to VULCAN [16], implying the TF's regulon is over-represented within the differentially bound genes. Importantly, qPLEX-RIME identified a significant increase in the protein-protein interaction between ER and GRHL2 in estrogenic conditions. As GRHL2 has a negative enrichment score in VULCAN, this implies either the protein is recruited by ER to sites that are significantly depleted for GRHL2's regulon or that GRHL2 is established as having a negative correlation to the genes regulated at these sites, i.e. the protein is a corepressor of the ER.

To assess the chromatin-association of ER and GRHL2, we undertook GRHL2 ChIP-seq in the absence (0 min) or presence (45 min) of E2 **(Figure 6A)**. VULCAN analysis of the GRHL2 differential binding showed that ER was the key interacting transcription factor, using both the TCGA- and METABRIC-derived networks **(Figure 6B)**.

We undertook a comparison of GRHL2 binding with public datasets **(Figure 6C).** Our analysis showed that GRHL2 sites that responded to estradiol were enriched for ER binding sites (in agreement with our qPLEX-RIME data and VULCAN results) and FOXA1 (compatible with either an ER interaction or the previously reported interaction with MLL3 [31]). Importantly, the changes in GRHL2 binding profiles after E2 treatment were not a result of altered GRHL2 protein levels **(Figure 7)**. Individual analysis of peaks show that classical ER promoter binding sites, e.g. RARa, were not the target of this redistribution of GRHL2, as these sites were occupied by GRHL2 before E2 stimulation. Motif analysis of the sites within increased GRHL2 occupancy showed enrichment for the full ERE (p-value = 1×10^{-179}) and the GRHL2 binding motif (p-value = 1×10^{-51}) **(Figure 6G)**.

To establish if the recruitment of GRHL2 was primarily related to a transcriptional function or the previously described interaction with MLL3, we overlapped our GRHL2 data with that of published H3K4me1/3 [31] and P300 [35] cistromes. While H3K4me occupancy was consistent between conditions, we found P300 binding to be enriched at the E2-responsive GRHL2 sites.

A more detailed analysis of the GRHL2 overlap with P300 sites showed the greatest co-occupancy of GRHL2/P300 sites was when both TFs were stimulated by E2 **(Figure 6D).** Moreover**,** overlap of GRHL2 peaks with ER ChIA-PET data [ENCSR000BZZ] showed that the

GRHL2 responsive sites were enriched at enhancers over promoters **(Figure 6E).** These findings suggested that the GRHL2-ER complex is involved in transcription at ER enhancer sites.

Validation of the ER-GRHL2 interaction by qPLEX-RIME and co-IP

qPLEX-RIME [34] analysis of GRHL2 in both the estrogen-free and estrogenic conditions (Supplementary File 4) showed high levels of transcription-related protein interactors including HDAC1 (p-value = 6.4×10^{-9}), TIF1A (p-value = 6.4×10^{-9}), PRMT (p-value = 6.4×10^{-9}) and GTF3C2 (p-value = 4.6×10^{-9}). P-values given for estrogen-free and estrogenic conditions conditions were comparable. The only protein differentially bound to GRHL2 in estrogen-free versus estrogenic conditions was the ER.

We further validated this interaction by co-IP. Our analysis robustly found that GRHL2 and ER interact in both MCF7 and T47D cells **(Figure 7).** We further validated the antibody by siRNA knockdown and saw the disappearance of the GRHL2 band at 24 hours.

GRHL2 constrains ER binding and activity

We investigated the transcription of enhancer RNAs at these sites using publicly available GRO-seq data [36] [GSE43836] **(Figure 6F).** At E2 responsive sites**,** eRNA transcription was strongly increased by E2 stimulation; by contrast, eRNA transcription was largely independent of E2 stimulation when the entire GRHL2 cistrome was considered. Analysis of a second GRO-seq dataset, GSE45822, corroborated these results **(Suppl. Figure S5-10)**.

To further explore how GRHL2 regulates ER enhancers, we measured eRNA expression at the GREB1 [37], [38], TFF1 [39]–[41] and XBP1 [42], [43] enhancers after over-expression of

GRHL2. At GREB1 and XBP1, increased GRHL2 resulted in reduced eRNA transcription **(Figure 8)** ($p < 0.05$, paired-sample, t-test). Conversely, eRNA production at the TFF1, XBP1 and GREB1 enhancers was moderately increased 24h after GRHL2 knockdown **(Suppl. Figure S6-2).** Combining data from all three sites established the effect as significant by paired-sample rank test ($p = 0.04$, one-tailed paired-sample, wilcoxon test). Collectively, these data demonstrate that GRHL2 constrains specific ER enhancer transcription.

A conserved alpha-helix between residues 425-437 of GRHL2 has previously been shown to inhibit P300 [44]. We therefore overexpressed GRHL2 Δ425-437, a previously demonstrated non-p300-inhibitory mutant [44], [45], in three ER positive breast cancer cell lines (MCF7, T47D and ZR75) and compared levels of eRNA to those recorded for both an empty vector control and for the over-expression of the wild type protein **(Figure 8B).** The results of the wild-type study were concordant to those of our previous analysis **(Figure 8A),** suggesting in general that overexpression GRHL2 leads to the inhibition of eRNA production at certain ER sites. Importantly, in all cases, the removal of aa 425-437 from GRHL2 led to a reduction in the inhibitory effect than caused by over-expression of the wild-type protein and was found as significant in 5 out of 9 cases test ($P < 0.05$, t-test, single-tail, paired).

We undertook H3K27ac ChIP-seq after knockdown of GRHL2 by siRNA for 48 hours. In both MCF7 and T47D cells, we saw a significant change in the acetylation marks surrounding GREB1, and in MCF7 we saw an increase at both XBP1 and GREB1 promoters and a decrease at TFF1 **(Figure 9A)**. Genome-wide, we saw a redistribution of H3K27 acetylation in both cell lines **(Figure 9B).** Comparison of the sites altered by GRHL2 knockdown showed a stronger signal for ER binding **(Figure 9C Right).**

Discussion

VirtUaL ChIP-seq Analysis through Networks – VULCAN

VULCAN is valuable for the discovery of transcription factors acting as coregulators within chromatin-bound complexes that would otherwise remain hidden. The challenge of highlighting cofactors from a ChIP-seq experiment lays in the infeasibility of reliable proteomic characterization of DNA-bound complexes at specific regions. On the other hand, while RNA-seq is arguably the most efficient technique to obtain genome-wide quantitative measurements, any transcriptomic approach cannot provide a full picture of cellular responses for stimuli that are provided on a shorter timescale than mRNA synthesis speed, such as the estradiol administration described in our study. VULCAN, by combining RNA-seq derived networks and ChIP-seq cistrome data, aims at overcoming limitations of both. Most notably, our method can work in scenarios where candidate cofactors do not have a well-characterized binding site or do not even bind DNA directly.

By developing VULCAN, we have been able to rediscover known cofactors of the estradiol-responsive ER complex and predict and experimentally validate a novel protein-protein interaction.

GRHL2-ER Interaction

GRHL2 has a key role in regulating EMT

In the 4T1 tumor model, GRHL2 was found to be significantly downregulated in cells that had undergone EMT [29]. The same study showed that knockdown of GRHL2 in MCF10A – an ER-negative cell line – led to loss of epithelial morphology. Overall, this suggested that the GRHL2 transcription factor plays an essential role in maintaining the epithelial phenotype of breast cells. Similar results were observed with the MDA-MB-231 model, where expression of GRHL2 resulted in reversal of EMT [30]. This result has been recapitulated in hepatocytes, where GRHL2 was found to suppress EMT by inhibiting P300 [44]. The ability to suppress EMT has also been noted in prostate cancer, another cancer driven by a steroid hormone receptor (AR), and the genes regulated by GRHL2 are linked to disease progression [46].

GRHL2 a novel corepressor of ER eRNA production

These earlier data combined with the link between GRHL2 expression and patient survival indicate a significant role for GRHL2 in the progression of breast cancer. However, its role in the ER signaling axis has, until now, been unknown. Here, we show that GRHL2 performs its activity at a subset of ER enhancers. Overexpression of GRHL2 resulted in a significant decrease in eRNA production at the TFF1 and XBP1 enhancers and, in agreement with previous studies that correlate eRNA transcription with gene expression [47]–[49], we found the measured eRNA decrease was concurrent with a significant downregulation in the expression of the corresponding gene.

These results are consistent with previous findings that GRHL2 inhibits P300 [44] and, while the ER complex results in the activation of eRNA transcription at these sites, that GRHL2 plays a role in fine-tuning or modulating this process.

GRHL2 role in the ER signaling axis is independent to its role in tethering MLL3

In breast cancer, GRHL2 has previously been shown to directly interact with FOXA1, which may contribute to tethering of the histone methyltransferase MLL3 and, consequently, epigenetic marks at GRHL2/FOXA1 binding sites [31]. Our analysis, however, showed no particular enrichment for H3K4me1/3 marks at E2 responsive GRHL2 sites compared to other GRHL2 binding sites and our proteomic analysis of interactors showed a strong association with proteins related to transcription. We proposed that these ER responsive sites are related to a role of GRHL2 in a transcriptional process independent of its interaction with MLL3. This was supported by evidence of a significant overlap with binding of the coactivator P300, transcriptional proteins detected by qPLEX-RIME analysis of GR, and a pronounced increase in eRNA transcription at E2 responsive GRHL2 sites.

ER is bound more strongly at active enhancers (H3K27ac) that are altered by siGRHL2

Knockdown of GRHL2 led to a genome-wide remodeling of H3K27ac marks, found at active enhancers, confirming a role of GRHL2 in partially regulating these sites. Detailed inspection of the data showed a significant increase of these marks around the XBP1 and GREB1 genes, supporting our hypothesis that GRHL2 has a partial inhibitory role within the ER regulon. The result was further supported by finding enrichment of ER binding events at H3K27ac marks altered by GRHL2 knockdown **(Figure 9C, Right Panel).** The more complex effect on H3K12ac, when compared to the effects on eRNA production, is likely a result of the diversity of roles that GRHL2 holds within the cell, leading to a host of downstream effects in the regulation of chromatin recruitment of key factors such as MLL3, ER and FOXA1[31]

Deletion of the P300 inhibitory α-helix from GRHL2 reduces the protein's ability to repress the production of eRNA at ER bound enhancer sites

Finally, to clarify if inhibition of P300 was occurring, we generated and overexpressed GRHL2 lacking the inhibitory alpha-helix at between amino acids 425-437. In all cases, GRHL2 Δ425-437 had reduced an inhibitory effect compared to overexpression of the wild-type, confirming that GRHL2 primarily plays a repressive role at these sites.

Conclusion

VULCAN is built on state-of-the-art network analysis tools previously applied to RNA-seq data. By adapting network-based strategies to ChIP-seq data, we have been able to reveal novel information regarding the regulation of breast cancer in a model system.

We have demonstrated that the VULCAN algorithm can be applied generally to ChIP-seq for the identification of new key regulator interactions. Our method provides a novel approach to investigate chromatin occupancy of cofactors that are too transient or for which no reliable antibody is available for direct ChIP-seq analysis.

Further, because of our use of clinical data, VULCAN results are both more likely to be relevant and are specific to the disease type studied, as demonstrated in the loss of signal when using a control coexpression network generated from an alternative disease type.

VULCAN enabled us to identify the GRHL2-ER interaction and that GRHL2 plays a repressive role. Further analysis showed the process to be independent to the previously reported interaction with FOXA1 and MLL3 [31]. Our conclusion, therefore, is that GRHL2 has a second, previously undescribed role that regulates transcription at specific estrogen responsive enhancers **(Figure 10)**.

Given the central role of the ER in breast cancer development and GRHL2's own ability to regulate EMT, the discovery that ER recruits GRHL2 leading to the altered eRNA production is an important step in enhancing our understanding of breast cancer and tumorigenesis.

Methods

VULCAN

An implementation of VULCAN in R is available on Bioconductor.org [https://bioconductor.org/packages/release/bioc/html/vulcan.html] and the scripts to replicate our analysis are available as a supplementary Rmarkdown file. Unless otherwise specified, all p-values were Bonferroni-corrected.

Sample preparation

MCF7 cells were obtained from the CRUK Cambridge Institute collection, authenticated by STR genotyping and confirmed free of mycoplasma. All cells were maintained at 37 ^{o}C, 5% CO_2. For each individual ChIP pull-down, we cultured 8 x 10^7 MCF7 cells (ATCC) across four 15 cm diameter plates in DMEM with 10% FBS, Glutamine and Penicillin/Streptomycin (Glibco). Five

days before the experiment, the cells were washed with phosphate buffered saline (PBS) and the media was replaced with clear DMEM supplemented with charcoal treated serum. The media was refreshed every 24 hours, which halted the growth of the cells and ensured that majority ER within the cell was not active. On day 5, the cells were treated with estradiol (100 nM). At the appropriate time point, the cells were washed with ice cold PBS twice and then fixed by incubating with 10mL per plate of 1% formaldehyde in unsupplemented clear media for 10 minutes. The reaction was stopped by the addition of 1.5mL of 2.5 M glycine and the plates were washed twice with ice cold PBS. Each plate was then scraped in 1 mL of PBS with protease inhibitors (PI) into a 1.5 mL microcentrifuge tube. The cells were centrifuged at 8000 rpm for 3 minutes at 4 ^{o}C and the supernatant removed. The process was repeated for a second wash in 1 mL PBS+PI and the PBS removed before storing at -80 ^{o}C.

ChIP-seq

Frozen samples were processed using established ChIP protocols [50] to obtain DNA fragments of ~300 bp in length. The libraries were prepared from the purified DNA using a Thruplex DNA-seq kit (Rubicon Genomics) and sequenced on the Illumina HiSeq Platform. Sequencing data is available from Gene Expression Omnibus, accession GSE109820 & GSE123475.

Differential binding analysis

Sequencing data was aligned using BWA [51] to the human genome (hg19). Reads from within the DAC Blacklisted Regions was removed before peak calling with MACS 2.1 [52] on default parameters. The aligned reads and associated peak files were then analyzed using DiffBind [18] to identify significant changes in ER binding.

Gene Set Enrichment Analysis (GSEA)

Gene Set Enrichment Analysis (GSEA) was performed as described by Subramanian et al. [53] using the curated pathway collection (C2) from MSIGDB v 5.0 with 1000 set permutations for each pathway investigated, followed by Benjamini Hochberg P-value correction.

Motif analysis

Motif analysis of the binding regions was undertaken with Homer v4.4 [54] using default parameters. Motif logo rendering was performed using Weblogo v2.8.2 [55]

VULCAN analysis

We reconstructed a regulatory gene network using ARACNe-AP as described by Alvarez [56]. RNA-seq breast cancer data was downloaded from TCGA on January 2015 and VST-Normalized as described by Anders and Huber [57]. The ARACNe transcriptional regulation network was imported into R using the VIPER BioConductor package and it was interrogated using the differential binding profiles from our ChIP-seq experiment as signatures, 45 minutes vs control and 90 minutes vs control. The peak-to-promoter assignment was performed using a 10kb window with respect to the transcription starting site (TSS) of every gene on the hg19 human genome. The algorithm msVIPER (multi-sample Virtual Inference of Protein activity by Enriched Regulon analysis) was then applied, leveraging the full set of eight replicates per group, with 1000 signature permutations and default parameters.

qPLEX-RIME

Samples were prepared as previously described for RIME [9], protocol was modified to include TMT isobaric labels for quantification [34]. qPLEX-RIME data and analysis pipeline is available as part of the supplementary Rmarkdown.

TF Binding Overlap

Publicly available data was downloaded as described in the source publication [3], [31], [35], [36] and overlap was calculated with bedtools (v2.25.0). Presented data was normalized as a percentage of GRHL2 sites.

Code availability

Code for data analysis is provided as a Rmarkdown document and supporting data is available from https://github.com/andrewholding/VULCANSupplementary. For convenience, we have provided VULCAN as a BioConductor package https://bioconductor.org/packages/release/bioc/html/vulcan.html along with a supporting data package https://bioconductor.org/packages/release/data/experiment/html/vulcandata.html.

eRNA quantification

MCF7 cells were transfected with Smart Pool siRNA (Dharmacon, L-014515-02), siControl, GRHL2 overexpression vector (Origene, RC214498), GRHL2 Δ425-437 (Origene), or empty

control vector using Lipofectamine 3000 (Thermo Fisher Scientific) according to the manufacturer's protocol in 6-well format. Expression was monitored by rtPCR using TaqMan assay with GAPDH as a control transcript. Knockdown efficiency was ~75% and the GRHL2 overexpression vector led a 730-fold increase in expression over control plasmid. 1 ug of purified RNA was reverse transcribed with Superscript III reverse transcriptase (Thermo Fisher Scientific, 18080085) using random primers (Promega, C1181) according to manufacturer instructions. eRNAs were quantified with qPCR using Power SYBR™ Green PCR Master Mix (Thermo Fisher Scientific, 4367660) and denoted as relative eRNA levels after normalizing with UBC mRNA levels.

Primer name	**Sequences**	**Reference**
eGREB1 F	ACTGCGGCATTTCTGTGAGA	This study
eGREB1 R	ACTGCAGTTTGCCTGTCACT	This study
eXBP1 F	TGTGAGCACTTGGCATCCAT	Nagarajan et al. 2014[58]
eXBP1 R	ACAGGGCCTCATTCTCCTCT	Nagarajan et al. 2014
eTFF1 F	AGGGGATGTGTGTGAGAAGG	Li et al. 2013[59]
eTFF1 R	GCTTCGAGACAGTGGGAGTC	Li et al. 2013
UBC F	ATTTGGGTCGCGGTTCTTG	Peña et al. 2006[60]
UBC R	TGCCTTGACATTCTCGATGGT	Peña et al. 2006

Co-Immunoprecipitation

ERα (F10) antibody, SantaCruz (sc-8002) was cleaned using Amicon 10K Buffer Exchange Column (EMD, Cat # UFC501096) to remove the Sodium Azide. 2.5 μ g ERα (F10) antibody rotated overnight at 4°C with 100μl Dynabeads Protein A, Invitrogen (10001D).

Nuclear lysate was harvested via cell lysis (20mM Tris-HCl, 20mM NaCl, 0.2mM EDTA) followed by nuclear lysis (20mM Tris-HCl, 20mM NaCl, 0.2mM EDTA 1% Igepal). Nuclear lysate was then incubated overnight at 4°C with the Dynabeads Protein A. Elution via 10 minutes incubation at 70°C with 1X NuPAGE LDS Sample Buffer, Invitrogen (NP0007) and 1X NuPAGE Sample Reducing Agent, Invitrogen (NP0004) and subjected to Western Blotting.

Knockdown of GRHL2

Knockdown of GRHL2 was undertaken using ON-TARGETplus SMARTpool Human GRHL2, Dharmacon (#L-014515-02-0050) and Lipofectamine® RNAiMAX Reagent Protocol (Thermo) according to the manufacturer's protocol. Control samples were prepared following the same method using ON-TARGETplus Control pool Non targeting pool, Dharmacon (#D-001810-10-50) in place of siGRHL2.

Author Contributions

ANH, FMG & LAS conceived and designed the experiments, ANH undertook ER experimentation, ANH & FMG undertook the analysis of ER data, ANH & FMG designed VULCAN, FMG

implemented the VULCAN analysis, AEC, ANH & AD undertook GRHL2 experimentation and SN undertook eRNA quantitation. ANH, AEC & LAS undertook analysis of GRHL2 data. ANH, FMG, AEC & LAS wrote the manuscript.

Acknowledgements

We would like to acknowledge the support of the University of Cambridge, Cancer Research UK and Hutchison Whampoa Limited.

Parts of this work were funded by CRUK core grant [grant numbers C14303/A17197, A19274] to FM; Breast Cancer Now Award [grant number 2012NovPR042] to FM and supported by The Alan Turing Institute under the EPSRC grant EP/N510129/129/1 as a Turing Fellowship to ANH.

We are grateful for the support of Eva Papachristou for undertaking the qPLEX-RIME analysis of our samples in advance of the her initial publication describing the method.

We would like to acknowledge the contribution from the CRUK Genomics, Proteomics and Bioinformatics core facilities in supporting this work.

Materials & Correspondence

All materials requests and correspondence should be addressed to Dr Andrew N. Holding.

Competing interests

The authors have no competing interests to declare.

Abbreviations

AR	Androgen Receptor
ARACNe-AP	AccuRate Algorithm for reConstruction of Network through Adaptive Partitioning
CCLE	Cancer Cell Line Encyclopedia
ChIP	Chromatin ImmunoPrecipitation
E2	Estradiol
ER	Estrogen Receptor-Alpha
ERE	Estrogen Response Elements
eRNA	Enhancer RNA
GSEA	Gene Set Enrichment Analysis
GRHL2	Grainyhead Like Transcription Factor 2
METABRIC	MolEcular TAxonomy of BReast cancer International Consortium
PBS	Phosphate Buffered Saline
PI	Protease Inhibitors
PR	Progesterone Receptor
TCGA	The Cancer Genome Atlas
TF	Transcription Factor
VIPER	Virtual Inference of Protein activity by Enriched Regulon analysis
VULCAN	VirtUaL ChIP-seq Analysis through Networks

Declarations

Parts of this work were funded by CRUK core grant C14303/A17197 and A19274 (to FM), and by Breast Cancer Now Award (2012NovPR042). None of the authors have any competing interests to declare. Data supporting this manuscript is available from the GEO accession GSE109820.

Figure Legends

Figure 1: An overview of VULCAN

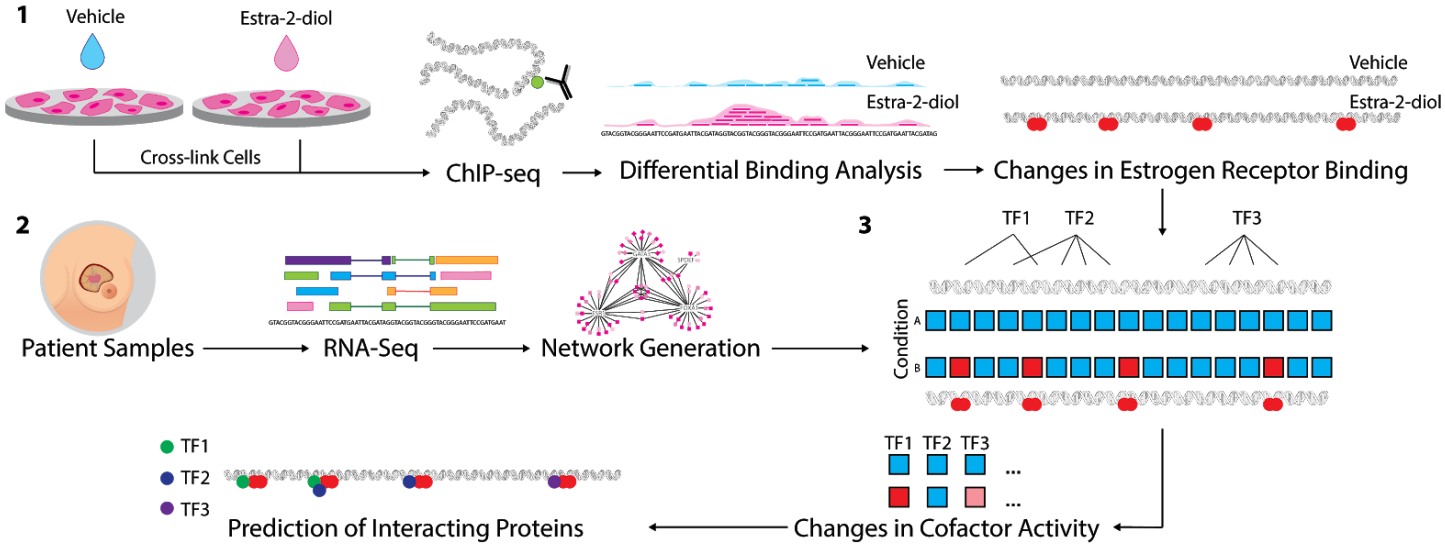

1.ChIP-seq analysis from multiple conditions is undertaken to generate cistrome data at multiple timepoints (or conditions). Binding events are then compared using differential binding analysis to establish log-fold change values for individual binding events between each timepoint. **2.** Network generation was undertaken with ARACNe-AP by inferring all pairwise TF-target coexpression from patient datasets (e.g. TCGA breast & METABRIC datasets). **3.** All the targets of each specific TF in the network, i.e. the individual regulons, are tested against the established changes in ER binding through the msVIPER algorithm[16] to identify proteins that interact with the target transcriptional factor and final prediction is given for potential interacting cofactors.

Figure 2: Dynamic behavior during early activation of ER

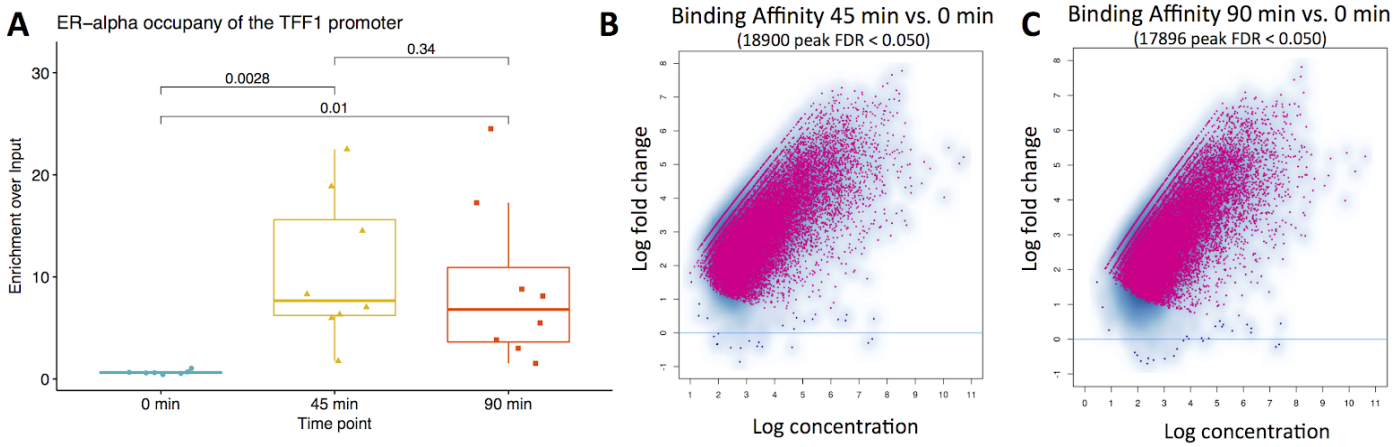

ChIP-qPCR of the TFF1 gene (A) at 3 timepoints shows increased binding of ER at 45 minutes after MCF7 cells are stimulated by estradiol. The previously reported maximum is followed by a decrease in the TFF1 promoter occupancy at 90 minutes. P-values are generated by one-tailed t-test. The maximal point at 90 minutes was identified as an outlier (> median + 2 x IQR); however, removal did not alter the significance of results. (B) Differential binding analysis of ChIP-seq data at three timepoints to monitor the activation of ER. The ER exhibits a strong increase in binding at 45 minutes vs 0 minutes (C) and the majority of sites still display binding at 90 minutes.

Figure 3: ER occupancy after estradiol treatment in terms of TF network activity

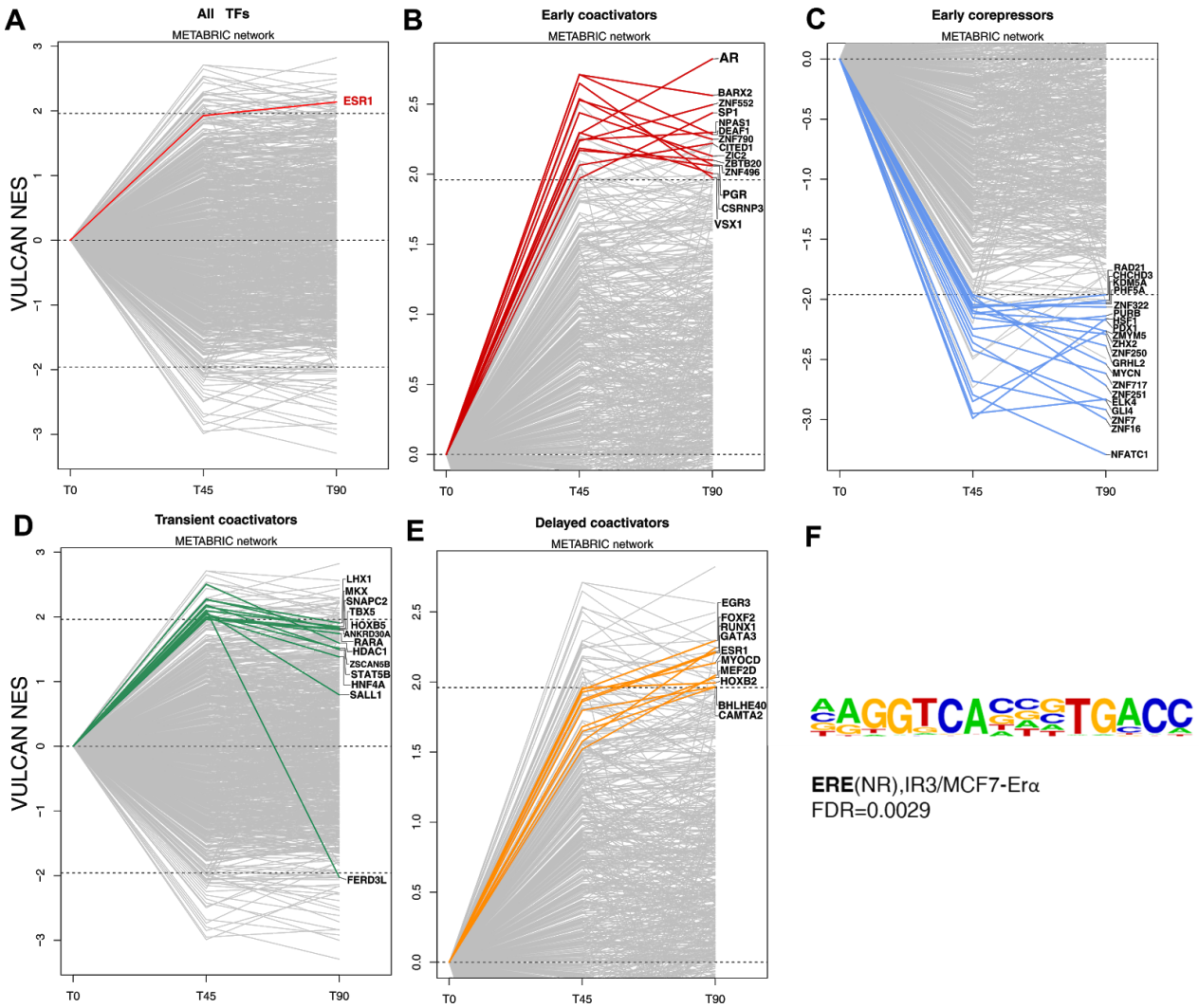

A: Global TF network behavior as predicted by VULCAN in our ChIP-seq dataset, highlighting the ESR1 TF at time 0 and 45/90 minutes after estradiol treatment.
B: Global TF activity after estradiol treatment in MCF7 cells, inferred using the METABRIC network, highlighting TFs significantly upregulated at 45 minutes and 90 minutes.
C: Global TF activity after estradiol treatment in MCF7 cells, inferred using the METABRIC network, highlighting TFs significantly downregulated at 45 minutes and 90 minutes.
D: Global TF activity after estradiol treatment in MCF7 cells, inferred using the METABRIC network, highlighting TFs significantly upregulated at 45 minutes but not at 90 minutes.
E: Global TF activity after estradiol treatment in MCF7 cells, inferred using the METABRIC network, highlighting TFs significantly upregulated at 90 minutes but not at 45 minutes.
F: Most enriched motif in peaks upregulated at both 45 and 90 minutes after estradiol treatment, as predicted by HOMER.

Figure 4: Global TF activity after estradiol treatment using different network models

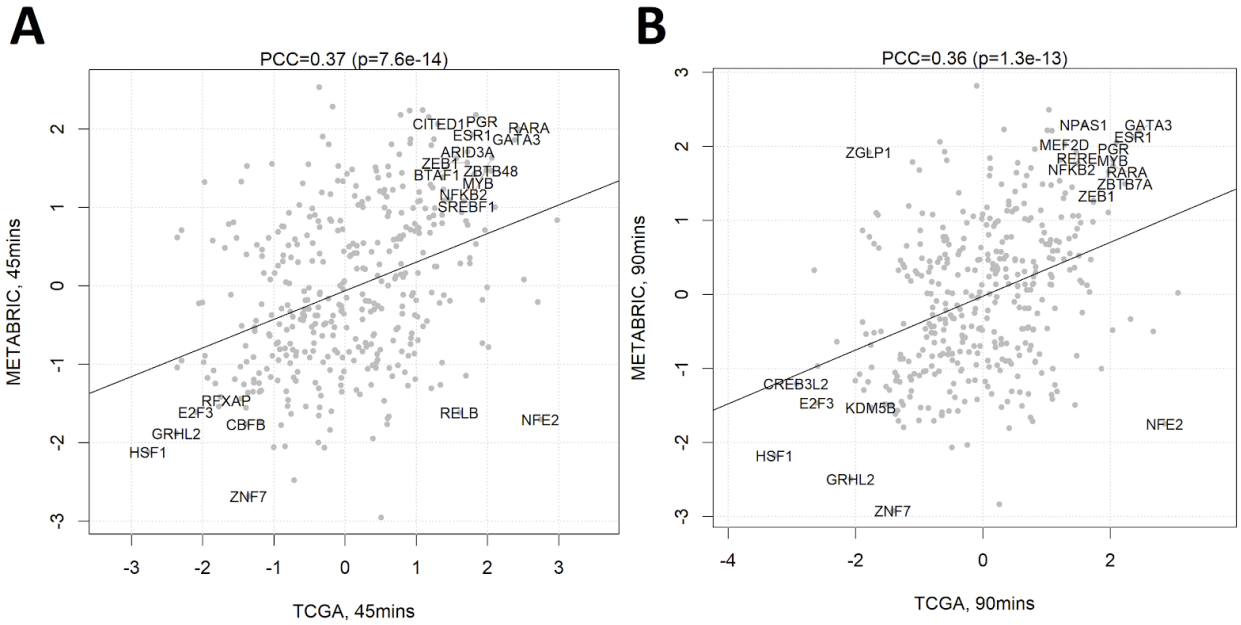

XY Scatter showing the TF activity as calculated by VULCAN for our differential ChIP-seq analysis of ER binding at 45 minutes (A) and at 90 minutes (B) after stimulation with 100 nM E2. Comparison of results calculated using the METABRIC (y-axis) and TCGA (x-axis) networks shows consistent results know ER interactors including PGR, RARA, GATA3 and GRHL2. GRHL2 activity is notably enriched against. The regulon of ER is also consistently enriched in both networks. Pearson's Correlation Coefficient (PCC) shown along with significance.

Figure 5: Inferring TF co-occupancy in public datasets with VULCAN

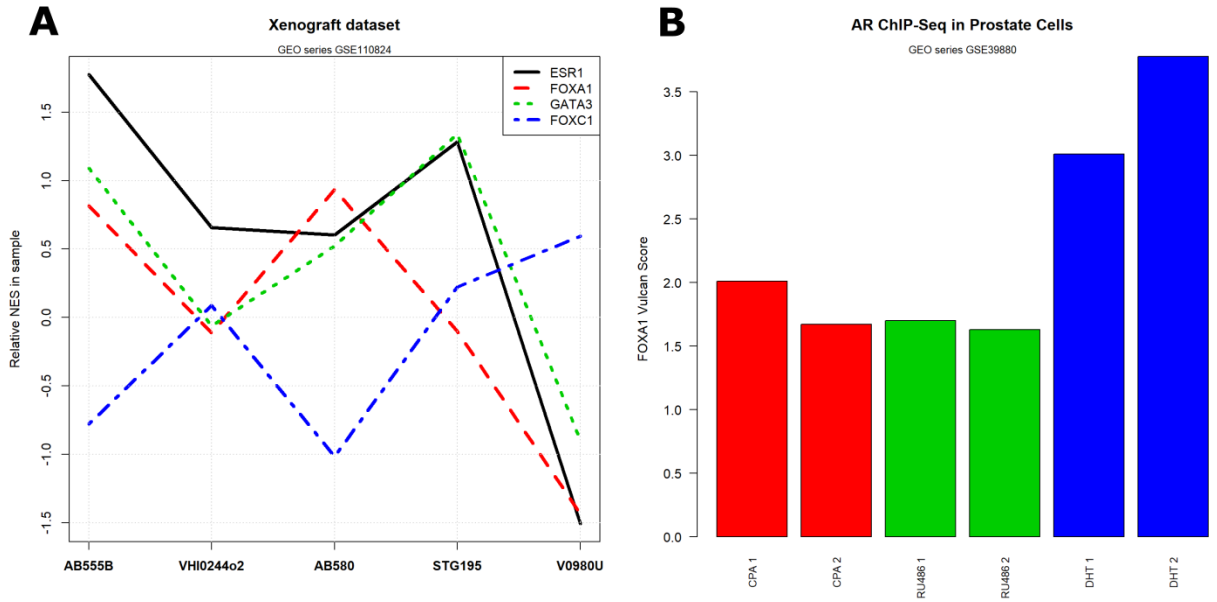

A. VULCAN Activity scores for a few TFs derived from the ER-targeted ChIP-seq Breast Cancer Patient-Derived Xenograft (PDX) dataset GSE110824. The behavior of ESR1, FOXA1 and GATA3 is correlated, while FOXC1 shows an inversely correlated pattern (blue line). Interestingly, the sample with the lowest Allred score (V0980U) has the lowest activity and the other luminal markers.

B. VULCAN Activity scores for FOXA1 in ChIP-seq experiments targeting the Androgen Receptor (AR) in LNCaP-1F5 prostate-derived cells (dataset GSE39880). The bar plots show the relative VULCAN Normalized Enrichment Score calculated on absolute peak intensities after treating cells with Dihydrotestosterone (DHT) and partial AR modulators cyproterone acetate (CPA) and Mifepristone (RU486). FOXA1 network binding is higher in the presence of the strong AR recruiter DHT. This shows an increased FOXA1/AR promoter co-occupancy in DHT-treated cells, in agreement with the conclusions of the study that originated the dataset. Two replicates for each treatment were produced and are reported in matching colors.

Figure 6: GRHL2 Differential ChIP-seq between 0 and 45 minutes

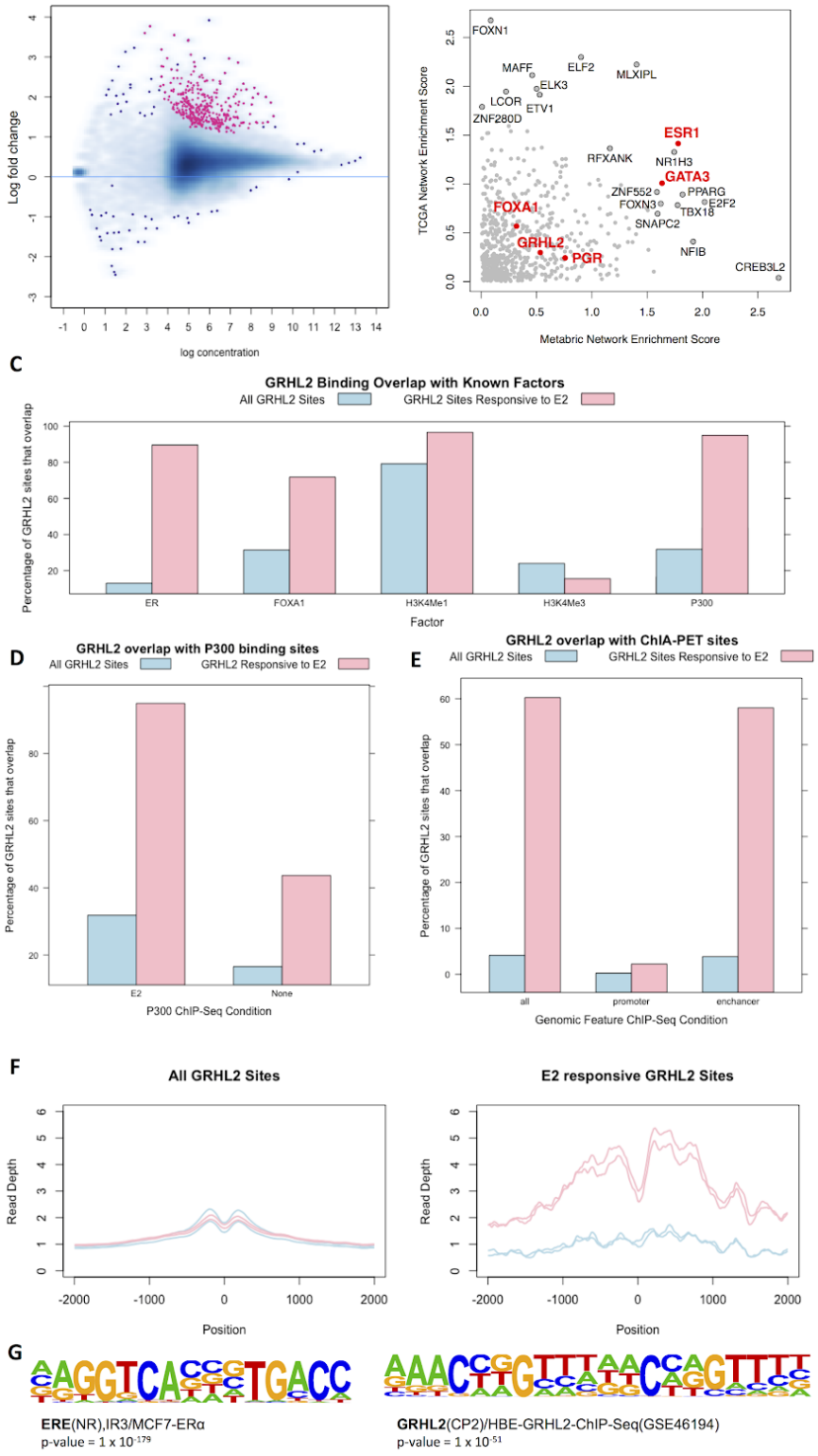

A. Activation of the ER with estro-2-diol results in a genome-wide increase in GRHL2 binding.
B. VULCAN Analysis of the same data show a significant enrichment for ESR1 sites in both the context of the METABRIC and TGCA networks. The regulon for FOXA1 is also not enriched. Inspection of known FOXA1/GRHL2 sites (e.g. RARa promoter) shows GRHL2 already bound.
C. Overlap of GRHL2 binding with public datasets shows that E2 responsive GRHL2 sites show considerable overlap with ER, FOXA1 and P300 sites, H3K4Me1 and H3K4Me3 show little enrichment.
D. Analysis of P300 binding showed a greater overlap of GRHL2 ER responsive sites in the presence of E2 than in control conditions.
E. Overlap with ER ChIA-PET sites showed enrichment for GRHL2 sites at ER enhancers.
F. Analysis of Gro-SEQ data (GSE43836) at GRHL2 sites. Blue lines are control samples, pink are samples after stimulation with E2. In general, GRHL2 sites (left) show no change in the levels of transcription on addition of E2; however, E2 responsive GRHL2 sites (right) show a robust increase in transcription on the activation of the ER.
G. Motif analysis of differentially bound sites gave the top two results as GRHL2 and ER.

Figure 7: Estrogen Time Course and Co-IP of GRHL2

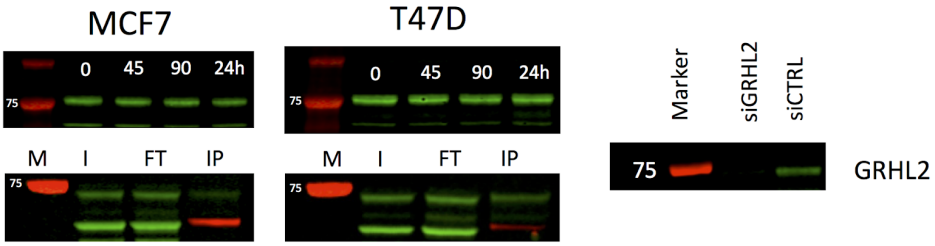

Analysis by western blot of the GRHL2 showed no changes in the levels of GRHL2 at 45 minutes, 90 minutes or 24 hours after stimulation with estradiol in either MCF7 or T47D. Co-IP of ER (bait, red, Santa Cruz:sc-8002) identified GRHL2 (green, Atlas: HPA004820) as an interactor in estrogenic conditions (M=Marker, I=Input, FT=Flow Through, IP=immunoprecipitation). siRNA knockdown of GRHL2 in MCF7 (right) resulted in loss of the ~75 kDa band.

Figure 8: Effect of GRHL2 knockdown after 24 hours on eRNA at E2 responsive binding sites & overexpression of GRHL2 Δ425-437

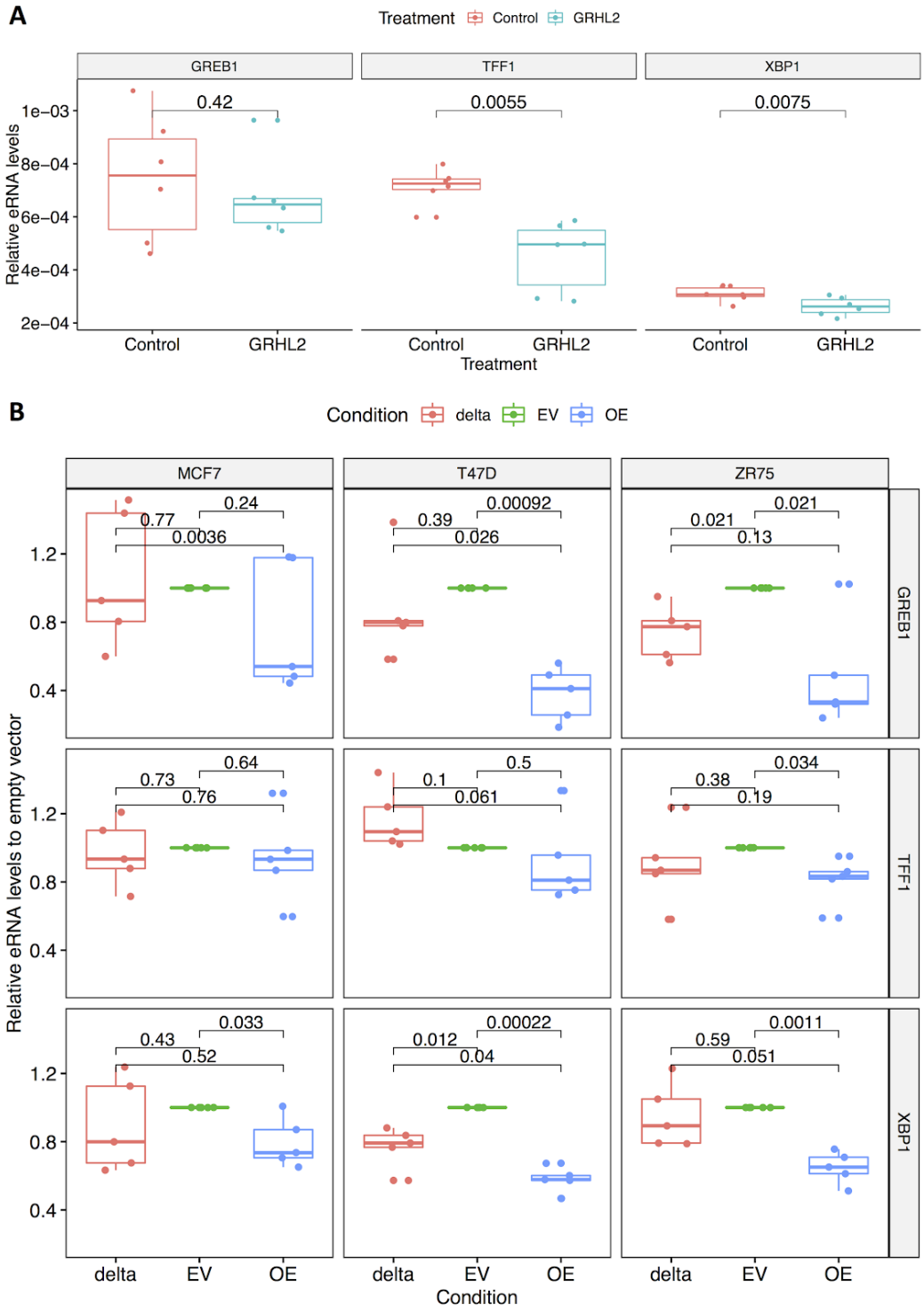

A. Overexpression of GRHL2 in MCF7 resulted in a reduction of eRNA transcribed from the GREB1, TFF1 and XBP1 enhancers. The effect was significant at TFF1 and XBP1 enhancers ($p < 0.05$, paired t-test).

B. Overexpression of GRHL2 Δ425-437 (delta) compared to empty vector (EV) and GRHL2 wild-type (OE) at 24 hours. In all 3 cell lines at all 3 loci, overexpression of the wild type (WT) led to a reduction in the mean eRNA production at GREB1, TFF1 and XPB1. This effect was significant in 6 out of 9 experiments ($P < 0.05$, t-test, one-tailed, paired). Overexpression of GRHL2 Δ425-437 had a reduced effect, that led to a significant reduction in only 2 out of 9 experiments ($P < 0.05$, t-test, one tailed, paired). Importantly, in 4 out of 9 experiments, WT overexpression had significantly less eRNA production than GRHL2 Δ425-437, suggesting the P300 inhibition domain plays a role in the regulation of eRNA production.

Figure 9: Changes in H3K27ac on knockdown of GRHL2

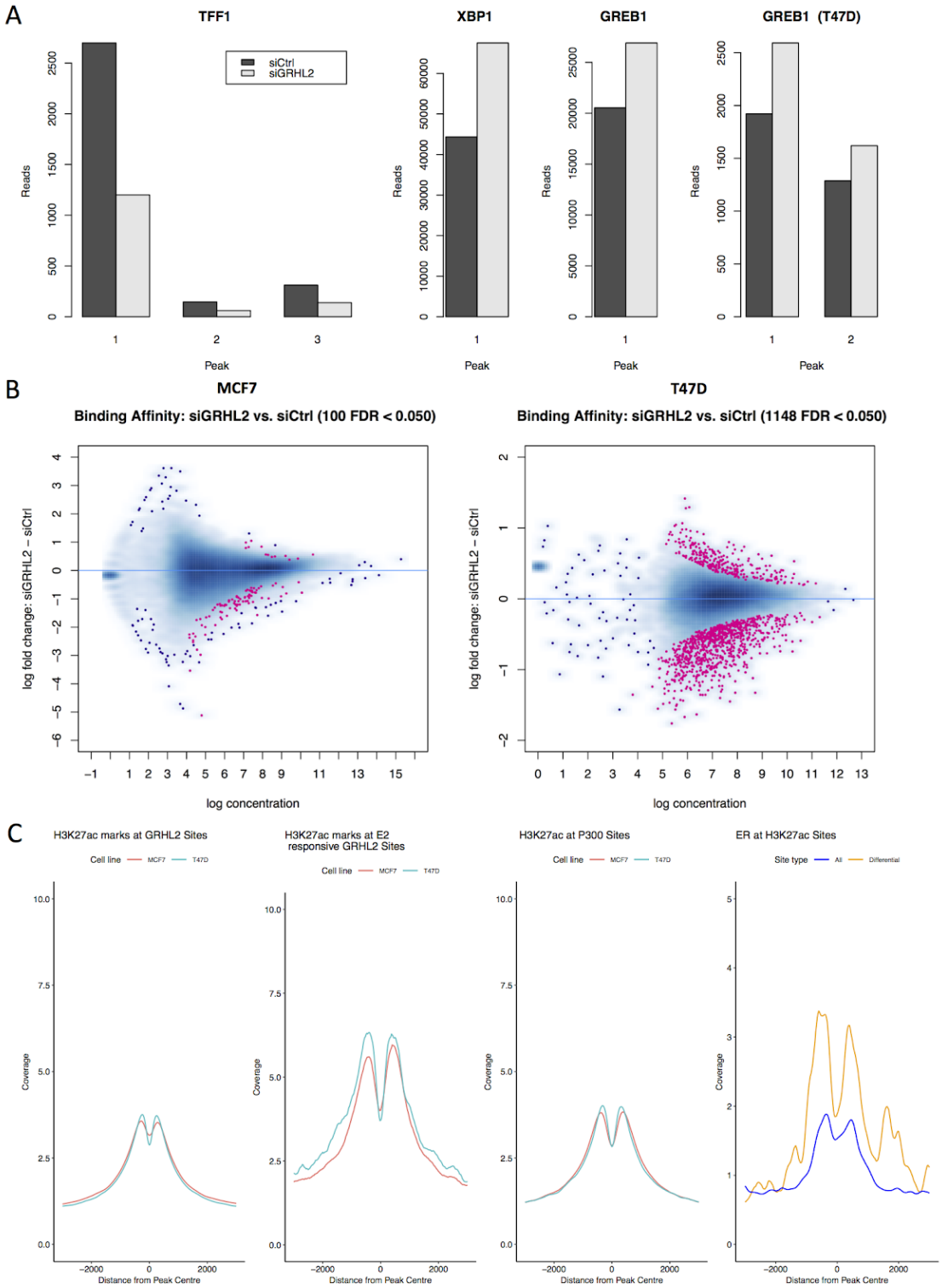

A. The effect of silencing GRHL2 on H3K27ac at 48 hours in MCF7 and T47D cell lines was monitored by ChIP-seq. Analysis of sites proximal to TFF1, XBP1 and GREB1 showed significant changes in acetylation at all three sites in MCF7. Significant changes were only found at GREB1 in T47D (top right). While XBP1 and GREB1 show an increase in histone acetylation on silencing GRHL2, TFF1 showed the reverse effect.

B. Genome-wide, the effects of silencing GRHL2 led to significant redistribution of H3K27ac in both the MCF7 and T47D cell lines, with both showing an increase and decrease in the histone mark dependent on site.

C. From left to right. Coverage as calculated by Homer. H3K27ac was found at GRHL2 sites in both MCF7 and T47D cells, in particular at the E2 responsive sites. The same mark was also found at P300 sites as expected. Analysis of ER binding at H3K27ac sites showed an enrichment for ER binding at the H3K27ac sites that were most responsive to knockdown of GRHL2 in MCF7 cells.

Figure 10: Overview of the role of GRHL2 in ER activation

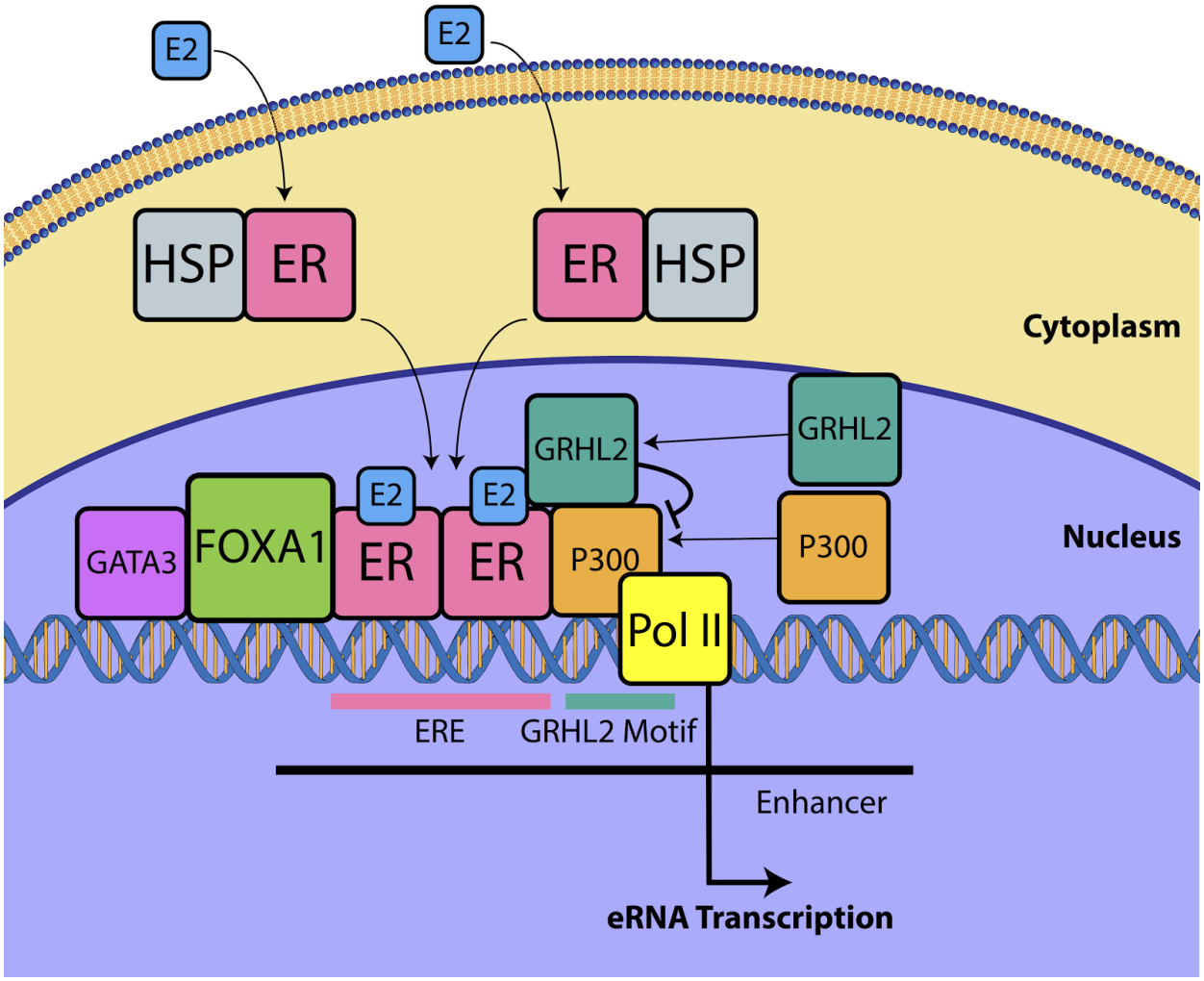

On activation of the ER by the ligand E2, the protein is released from a complex containing HSPs and translocates to the nucleus. The holo-ER dimer forms a core complex at Estrogen Response Elements (ERE) with FOXA1 (pioneer factor) and GATA3. ER further recruits P300 and GRHL2. GRHL2 has an inhibitory effect on P300 (a transcriptional activator interacting with TFIID, TFIIB, and RNAPII), thereby reducing the level of eRNA transcription at enhancer sites. Overexpression of GRHL2 further suppresses transcription, while knockdown of GRHL2 reverses the process.

References:

[1] R. L. Siegel, K. D. Miller, and A. Jemal, “Cancer statistics, 2018.,” CA: Cancer J. Clin., vol. 68, no. 1, pp. 7–30, Jan. 2018.

[2] K. S. Zaret and J. S. Carroll, “Pioneer transcription factors: establishing competence for gene expression.,” Genes & Dev., vol. 25, no. 21, pp. 2227–2241, Nov. 2011.

[3] A. Hurtado, K. A. Holmes, C. S. Ross-Innes, D. Schmidt, and J. S. Carroll, “FOXA1 is a key determinant of estrogen receptor function and endocrine response,” Nat Genet., vol. 43, pp. 27–33, 2010.

[4] K. B. Horwitz, T. A. Jackson, D. L. Bain, J. K. Richer, G. S. Takimoto, and L. Tung, “Nuclear receptor coactivators and corepressors.,” Mol. Endocrinol., vol. 10, no. 10, Oct. 1996.

[5] C. K. Glass, D. W. Rose, and M. G. Rosenfeld, “Nuclear receptor coactivators.,” Curr. Opin. cell Biol., vol. 9, no. 2, pp. 222–232, Apr. 1997.

[6] K. A. Green and J. S. Carroll, “Oestrogen-receptor-mediated transcription and the influence of co-factors and chromatin state.,” Nat. Rev. Cancer, vol. 7, no. 9, pp. 713–722, Sep. 2007.

[7] H. Nakshatri and S. Badve, “FOXA1 as a therapeutic target for breast cancer.,” Expert Opin. Ther. targets, vol. 11, no. 4, pp. 507–514, Apr. 2007.

[8] Y. Wu et al., “Tamoxifen Resistance in Breast Cancer Is Regulated by the EZH2-ERα-GREB1 Transcriptional Axis.,” Cancer Res., vol. 78, no. 3, pp. 671–684, Feb. 2018.

[9] H. Mohammed et al., “Endogenous purification reveals GREB1 as a key estrogen receptor regulatory factor.,” Cell reports, vol. 3, no. 2, pp. 342–349, Feb. 2013.

[10] C. I. Wang et al., “Chromatin proteins captured by ChIP-mass spectrometry are linked to dosage compensation in Drosophila.,” Nat. Struct. & Mol. Biol., vol. 20, no. 2, pp. 202–209, Feb. 2013.

[11] E. L. Hong et al., “Principles of metadata organization at the ENCODE data coordination center.,” Database̊: J. Biol. databases Curation, vol. 2016, Mar. 2016.

[12] C. Y. McLean et al., “GREAT improves functional interpretation of cis-regulatory regions.,” Nat. Biotechnol., vol. 28, no. 5, pp. 495–501, May 2010.

[13] R. P. Welch et al., “ChIP-Enrich: gene set enrichment testing for ChIP-seq data.,” Nucleic acids Res., vol. 42, no. 13, p. e105, Jul. 2014.

[14] P. J. Balwierz, M. Pachkov, P. Arnold, A. J. Gruber, M. Zavolan, and E. van Nimwegen, “ISMARA: automated modeling of genomic signals as a democracy of regulatory motifs.,” Genome Res., vol. 24, no. 5, pp. 869–884, May 2014.

[15] A. Subramanian et al., “Gene set enrichment analysis: a knowledge-based approach for interpreting genome-wide expression profiles.,” Proc. Natl. Acad. Sci. United States Am., vol. 102, no. 43, pp. 15545–15550, Oct. 2005.

[16] M. J. Alvarez et al., “Functional characterization of somatic mutations in cancer using network-based inference of protein activity.,” Nat. Genet., vol. 48, no. 8, pp. 838–847, Aug. 2016.

[17] A. N. Holding, A. E. Cullen, and F. Markowetz, “Genome-wide Estrogen Receptor-alpha activation is sustained, not cyclical,” bioRxiv, Jan. 2018.

[18] C. S. Ross-Innes et al., “Differential oestrogen receptor binding is associated with clinical outcome in breast cancer.,” Nature, vol. 481, no. 7381, pp. 389–393, Jan. 2012.

[19] R. A. Stein et al., “Estrogen-related receptor alpha is critical for the growth of estrogen

receptor-negative breast cancer.," Cancer Res., vol. 68, no. 21, pp. 8805–8812, Nov. 2008.
[20] P. Bhat-Nakshatri et al., "AKT alters genome-wide estrogen receptor alpha binding and impacts estrogen signaling in breast cancer.," Mol. Cell. Biol., vol. 28, no. 24, pp. 7487–7503, Dec. 2008.
[21] J. M. Gozgit, B. T. Pentecost, S. A. Marconi, R. S. J. Ricketts-Loriaux, C. N. Otis, and K. F. Arcaro, "PLD1 is overexpressed in an ER-negative MCF-7 cell line variant and a subset of phospho-Akt-negative breast carcinomas.," Br. J. Cancer, vol. 97, no. 6, pp. 809–817, Sep. 2007.
[22] M. J. Guertin, A. E. Cullen, F. Markowetz, and A. N. Holding, "Parallel factor ChIP provides essential internal control for quantitative differential ChIP-seq.," Nucleic acids Res., vol. 46, no. 12, p. e75, Jul. 2018.
[23] A. Bruna et al., "A Biobank of Breast Cancer Explants with Preserved Intra-tumor Heterogeneity to Screen Anticancer Compounds.," Cell, vol. 167, no. 1, p. 260–274.e22, Sep. 2016.
[24] B. Sahu et al., "FoxA1 specifies unique androgen and glucocorticoid receptor binding events in prostate cancer cells.," Cancer Res., vol. 73, no. 5, pp. 1570–1580, Mar. 2013.
[25] B. Sahu et al., "Dual role of FoxA1 in androgen receptor binding to chromatin, androgen signalling and prostate cancer.," EMBO J., vol. 30, no. 19, pp. 3962–3976, Sep. 2011.
[26] "Retrieving publications from Library." .
[27] D. Wang et al., "Reprogramming transcription by distinct classes of enhancers functionally defined by eRNA.," Nature, vol. 474, no. 7351, pp. 390–394, May 2011.
[28] A. Liberzon, A. Subramanian, R. Pinchback, H. Thorvaldsdottir, P. Tamayo, and J. P. Mesirov, "Molecular signatures database (MSigDB) 3.0," Bioinformatics, vol. 27, no. 12, Jun. 2011.
[29] X. Xiang et al., "Grhl2 determines the epithelial phenotype of breast cancers and promotes tumor progression.," PloS one, vol. 7, no. 12, p. e50781, Dec. 2012.
[30] B. Cieply et al., "Suppression of the epithelial-mesenchymal transition by Grainyhead-like-2.," Cancer Res., vol. 72, no. 9, pp. 2440–2453, May 2012.
[31] K. M. Jozwik, I. Chernukhin, A. A. Serandour, S. Nagarajan, and J. S. Carroll, "FOXA1 Directs H3K4 Monomethylation at Enhancers via Recruitment of the Methyltransferase MLL3.," Cell reports, vol. 17, no. 10, pp. 2715–2723, Dec. 2016.
[32] K. T. Helzer et al., "The Phosphorylated Estrogen Receptor Cistrome Identifies a Subset of Active Enhancers Enriched for Direct ER-DNA Binding and the Transcription Factor GRHL2.," Mol. Cell. Biol., Nov. 2018.
[33] A. Thompson et al., "Tandem Mass Tags: A Novel Quantification Strategy for Comparative Analysis of Complex Protein Mixtures by MS/MS," Anal. Chem., vol. 75, no. 18, Sep. 2003.
[34] E. K. Papachristou et al., "A quantitative mass spectrometry-based approach to monitor the dynamics of endogenous chromatin-associated protein complexes.," Nat. Commun., vol. 9, no. 1, p. 2311, Jun. 2018.
[35] W. Zwart, V. Theodorou, M. Kok, S. Canisius, S. Linn, and J. S. Carroll, "Oestrogen receptor-co-factor-chromatin specificity in the transcriptional regulation of breast cancer.," EMBO J., vol. 30, no. 23, pp. 4764–4776, Oct. 2011.
[36] N. Hah, S. Murakami, A. Nagari, C. G. Danko, and W. L. Kraus, "Enhancer transcripts mark active estrogen receptor binding sites.," Genome Res., vol. 23, no. 8, pp. 1210–1223, Aug. 2013.
[37] M. G. Ghosh, D. A. Thompson, and R. J. Weigel, "PDZK1 and GREB1 are estrogen-regulated genes expressed in hormone-responsive breast cancer.," Cancer Res., vol. 60, no. 22, pp. 6367–6375, Nov. 2000.
[38] J. M. Rae, M. D. Johnson, J. O. Scheys, K. E. Cordero, J. M. Larios, and M. E. Lippman,

"GREB 1 is a critical regulator of hormone dependent breast cancer growth.," Breast Cancer Res. Treat., vol. 92, no. 2, pp. 141–149, Jul. 2005.
[39] S. J. Prest, F. E. B. May, and B. R. Westley, "The estrogen-regulated protein, TFF1, stimulates migration of human breast cancer cells.," FASEB J.: Off. Publ. Fed. Am. Soc. Exp. Biol., vol. 16, no. 6, pp. 592–594, Apr. 2002.
[40] S. Ribieras, C. Tomasetto, and M. C. Rio, "The pS2/TFF1 trefoil factor, from basic research to clinical applications.," Biochim. et Biophys. Acta, vol. 1378, no. 1, pp. F61–F77, Aug. 1998.
[41] M. Crosier, D. Scott, R. G. Wilson, C. D. Griffiths, F. E. May, and B. R. Westley, "High expression of the trefoil protein TFF1 in interval breast cancers.," Am. J. Pathol., vol. 159, no. 1, pp. 215–221, Jul. 2001.
[42] M. Lacroix and G. Leclercq, "About GATA3, HNF3A, and XBP1, three genes co-expressed with the oestrogen receptor-alpha gene (ESR1) in breast cancer.," Mol. Cell. Endocrinol., vol. 219, no. 1–2, pp. 1–7, Apr. 2004.
[43] D. S. Oh, "Estrogen-Regulated Genes Predict Survival in Hormone Receptor-Positive Breast Cancers," J. Clin. Oncol., vol. 24, no. 11, Feb. 2006.
[44] P. M. Pifer et al., "Grainyhead-like 2 inhibits the coactivator p300, suppressing tubulogenesis and the epithelial-mesenchymal transition.," Mol. Biol. cell, vol. 27, no. 15, pp. 2479–2492, Aug. 2016.
[45] I. MacFawn et al., "Grainyhead-like-2 confers NK-sensitivity through interactions with epigenetic modifiers.," Mol. Immunol., vol. 105, pp. 137–149, Jan. 2019.
[46] S. Paltoglou et al., "Novel Androgen Receptor Coregulator GRHL2 Exerts Both Oncogenic and Antimetastatic Functions in Prostate Cancer.," Cancer Res., vol. 77, no. 13, pp. 3417–3430, Jul. 2017.
[47] J.-H. Cheng, D. Z.-C. Pan, Z. T.-Y. Tsai, and H.-K. Tsai, "Genome-wide analysis of enhancer RNA in gene regulation across 12 mouse tissues.," Sci. reports, vol. 5, p. 12648, Jul. 2015.
[48] S. Rahman et al., "Single-cell profiling reveals that eRNA accumulation at enhancer-promoter loops is not required to sustain transcription.," Nucleic acids Res., vol. 45, no. 6, pp. 3017–3030, Apr. 2017.
[49] T.-K. Kim et al., "Widespread transcription at neuronal activity-regulated enhancers.," Nature, vol. 465, no. 7295, pp. 182–187, May 2010.
[50] K. A. Holmes, G. D. Brown, and J. S. Carroll, "Chromatin Immunoprecipitation-Sequencing (ChIP-seq) for Mapping of Estrogen Receptor-Chromatin Interactions in Breast Cancer.," Methods Mol. Biol., vol. 1366, pp. 79–98, 2016.
[51] H. Li and R. Durbin, "Fast and accurate short read alignment with Burrows-Wheeler transform," Bioinformatics, vol. 25, no. 14, Jul. 2009.
[52] Y. Zhang et al., "Model-based analysis of ChIP-Seq (MACS)," Genome Biol., vol. 9, no. 9, p. 137, 2008.
[53] A. Subramanian et al., "Gene set enrichment analysis: a knowledge-based approach for interpreting genome-wide expression profiles: a knowledge-based approach for interpreting genome-wide expression profiles.," Proc. Natl. Acad. Sci. United States Am., vol. 102, no. 43, pp. 15545–15550, Oct. 2005.
[54] S. Heinz et al., "Simple combinations of lineage-determining transcription factors prime cis-regulatory elements required for macrophage and B cell identities.," Mol. cell, vol. 38, no. 4, pp. 576–589, May 2010.
[55] G. E. Crooks, G. Hon, J.-M. Chandonia, and S. E. Brenner, "WebLogo: a sequence logo generator.," Genome Res., vol. 14, no. 6, pp. 1188–1190, Jun. 2004.
[56] A. Lachmann, F. M. Giorgi, G. Lopez, and A. Califano, "ARACNe-AP: gene network reverse

engineering through adaptive partitioning inference of mutual information," Bioinformatics, vol. 32, no. 14, Jul. 2016.
[57] S. Anders and W. Huber, "Differential expression analysis for sequence count data.," Genome Biol., vol. 11, p. 106, Jan. 2010.
[58] S. Nagarajan et al., "Bromodomain protein BRD4 is required for estrogen receptor-dependent enhancer activation and gene transcription.," Cell reports, vol. 8, no. 2, pp. 460–469, Jul. 2014.
[59] W. Li et al., "Functional roles of enhancer RNAs for oestrogen-dependent transcriptional activation.," Nature, vol. 498, no. 7455, pp. 516–520, Jun. 2013.
[60] C. Peña et al., "The expression levels of the transcriptional regulators p300 and CtBP modulate the correlations between SNAIL, ZEB1, E-cadherin and vitamin D receptor in human colon carcinomas.," Int. J. Cancer, vol. 119, no. 9, pp. 2098–2104, Nov. 2006.